Journal of Catalysis 258 (2008) 103–110

Contents lists available at ScienceDirect

Journal of Catalysis

www.elsevier.com/locate/jcat

Surface chemistry and reactivity of well-defined multilayered supported $M_1O_x/M_2O_x/SiO_2$ catalysts

Edward L. Lee, Israel E. Wachs *

Operando Molecular Spectroscopy and Catalysis Laboratory, Chemical Engineering Department, 111 Research Drive, Iacocca Hall, Lehigh University, Bethlehem, PA 18015, USA

ARTICLE INFO

Article history:
Received 19 March 2008
Revised 30 May 2008
Accepted 3 June 2008
Available online 17 July 2008

Keywords:
Catalysts
Supported
SiO_2
Oxides
V_2O_5
CrO_3
MoO_3
WO_3
Re_2O_7
Reactivity
Kinetics
Temperature programmed surface reaction
TPSR
CH_3OH
HCHO
CH_3OCH_3
CO
CO_2

ABSTRACT

A series of group 5–7 transition metal oxides (TMOs) were supported on SiO_2 and surface-modified SiO_2 containing surface AlO_x, ZrO_x, and TiO_x species. The surface reactivity of these silica supported oxides was chemically probed with CH_3OH-temperature-programmed surface reaction (TPSR) spectroscopy. The selectivity of the model supported MO_x catalytic active sites on SiO_2 generally reflect the same product distribution as their corresponding bulk MO_x counterparts toward dimethyl ether (DME), formaldehyde (HCHO) and CO_2 from surface acidic, redox, and basic sites, respectively. The reactivity of the surface MO_x sites generally was suppressed by anchoring of the surface MO_x species onto the SiO_2 support. The general surface chemistry trend followed the known inorganic chemistry of the corresponding bulk MO_x TMOs. For the multilayered supported $M_1O_x/M_2O_x/SiO_2$, with M_1 representing the group 5–7 TMOs and M_2 representing Al, Zr or Ti, the selectivity of the catalytic active sites was generally comparable to that for the model-supported M_1O_x/SiO_2 catalysts. The reactivity of the surface VO_x, MoO_x, and ReO_x redox sites increased by one to four orders of magnitude with the introduction of the surface modifiers; however, the reactivity of the surface WO_x acidic site was mildly suppressed by the presence of the surface modifiers. The reactivity of the basic CrO_x site was only mildly perturbed by the surface modifiers. The reactivity trend of the catalytic TMOs sites was related to the electronegativity properties of the anchoring substrate cations (Si > Al > Zr ~ Ti).

1. Introduction

Various promoters or additives are generally added to the supported MO_x/SiO_2 catalyst systems to enhance their catalytic performance (e.g., enhanced activity, improved selectivity, thermal stability). Some of the typical additives are oxides of AlO_x, ZrO_x, and TiO_x. The interaction between Al_2O_3–SiO_2 generates new Brønsted acidic sites at bridging Al–OH–Si bond [1]. The ZrO_2–SiO_2 interaction also results in enhanced surface acidity, as well as excellent chemical resistance to alkaline corrosion and low thermal expansion [2], and the interaction between TiO_2–SiO_2 also yields high thermal stability, excellent mechanical strength, and generation of new catalytic active acidic sites [3]. These surface-modified SiO_2 mixed oxides are further used as oxide supports for the supported group 5–7 transition metal oxide catalysts. The literature reports various industrial applications for these supported catalysts, including ammoxidation of 3-picoline (V_2O_5/Al_2O_3–SiO_2) [4], selective catalytic reduction (SCR) of nitrogen oxide with ammonia and NO reduction with CO ($V_2O_5/TiO_2/SiO_2$) [3,5–11], ethylene polymerization (CrO_3/TiO_2–SiO_2) [12,13], denitrogenation of nitrogen containing heteroaromatic compounds (Mo/Al_2O_3–SiO_2) [14,15], HDS of thiophene (Mo/ZrO_2–SiO_2 and MoO_3/TiO_2–SiO_2) [16–18], and alkene metathesis and epoxidation with H_2O_2 (Re_2O_7/Al_2O_3–SiO_2) [19,20]. These promoted mixed-oxide support materials have been found to have more favorable catalytic properties than the more conventional supported MO_x/SiO_2 catalysts.

The molecular and electronic structures of the supported group 5–7 transition metal oxides on SiO_2 and surface modified SiO_2 (where surface modification is achieved with surface AlO_x, ZrO_x, and TiO_x species) have been successfully determined [21–23]. The group 5 metal oxides maintain the monoxo surface structure (M=O) for both the native SiO_2 and the surface modified SiO_2 supports. The surface monoxo (M=O)/dioxo ($M(=O)_2$) ratio of the

* Corresponding author. Fax: +1 (610) 758 6555.
E-mail address: iew0@lehigh.edu (I.E. Wachs).

0021-9517/$ – see front matter
doi:10.1016/j.jcat.2008.06.002

group 6 metal oxides (CrO_x, MoO_x, and WO_x) is controlled by the surface modifiers, however. The group 7 metal oxide of surface ReO_4 maintains the trioxo structure ($Re(=O)_3$) in the presence and absence of the surface modifiers. The promoters also have a significant effect on the corresponding electronic structure and result in a narrower distribution of isolated surface metal oxide species, especially for the group 6 metal oxides. These structural changes in the surface species also demonstrate that the surface group 5–7 transition metal oxides preferentially anchor to the surface modifiers (AlO_x, ZrO_x, and TiO_x) over the exposed SiO_2 support sites.

The objective of this investigation was to determine the influence of the surface modifiers on the molecular/electronic structure-activity/selectivity relationships for the multilayered SiO_2-supported group 5–7 metal oxide catalysts. Surface AlO_x, ZrO_x, and TiO_x species were used as the surface modifiers in this study. The surface chemistry and reactivity was chemically probed with CH_3OH-temperature-programmed surface reaction (TPSR) spectroscopy. The CH_3OH-TPSR experiments provide information about the nature of the catalytic active sites (redox, acidic, or basic) and their specific surface reactivity (k_{rds}) toward methanol, in which k_{rds} represents the first-order kinetic constant of the rate-determining-step (RDS) [24–27]. The catalytic activities of the model supported MO_x/SiO_2 catalyst systems were assessed and used as benchmarks for the multilayered supported metal oxide catalysts.

2. Experimental

2.1. Catalyst synthesis

The SiO_2-supported catalysts consist of highly dispersed metal oxides (Al_2O_3, TiO_2, ZrO_2, V_2O_5, CrO_3, MoO_3, WO_3, and Re_2O_7) that were successfully prepared by incipient wetness impregnation, as described in detail elsewhere [21,28–30]. The SiO_2 support material, amorphous SiO_2 (Cabot, Cab–O–Sil fumed silica EH-5, S.A. = 332 m^2/g), was found to be more easily handled by an initial water pretreatment and calcination at 500 °C for 4 h with no change in the material properties. The SiO_2 support was impregnated with aqueous and nonaqueous (toluene) solutions of the corresponding precursors: aluminum sec-butoxide ($Al[O(CH_3)CH_2H_5]_3$, Alfa Aesar, 95%), titanium isopropoxide ($Ti[OCH(CH_3)_2]_4$, Alfa-Aesar, 99.999%), zirconium tert-butoxide ($Zr[OC(CH_3)_3]_4$, Alfa Aesar, 97%), vanadium triisopropoxide ($VO[CHO(CH_3)_2]_3$, Alfa Aesar, 97%), chromium (III) nitrate ($Cr(NO_3)_3{\cdot}9H_2O$, Alfa Aesar, 98.5%), ammonium heptamolybdate ($(NH_4)_6Mo_7O_{24}{\cdot}4H_2O$, Aldrich, 99.98%), ammonium metatungstate ($(NH_4)_6H_2W_{12}O_{40}{\cdot}xH_2O$, Pfaltz and Bauer, 99.5%), or perrhenic acid ($HReO_4$, Alfa Aesar, 75–80%). The SiO_2 was initially dried for 2 h at 115 °C for the nonaqueous preparations before synthesis inside a glove box (Vacuum Atmospheres, Omni-Lab VAC 101965) under a nitrogen environment. After impregnation, the samples were allowed to dry overnight under the nitrogen atmosphere. Calcination of the samples entailed ramping at 1 °C/min to 110 °C and holding for 5 h under flowing N_2 (Airgas, ultra-high purity) in a programmable furnace (Thermolyne model 48000), followed by another 1 °C/min ramp under flowing air (Airgas, Zero grade) to 500 °C (with 450 °C used for the V_2O_5/SiO_2, in keeping with earlier studies) and holding for 6 h. The procedure for the aqueous preparations was the same as for the nonaqueous preparations, except that the drying and initial calcination steps were performed in ambient air and under flowing air (Airgas, zero grade), respectively. The surface modified SiO_2 supports, Al_2O_3/SiO_2, TiO_2/SiO_2, and ZrO_2/SiO_2, were synthesized with 5 wt% metal oxide loadings on SiO_2. The model catalysts, V_2O_5/SiO_2, CrO_3/SiO_2, MoO_3/SiO_2, WO_3/SiO_2, and Re_2O_7/SiO_2, were synthesized with 3 wt% metal oxides on SiO_2 (with 5 wt% used for V_2O_5/SiO_2, in keeping with earlier studies), henceforth designated MO_x/SiO_2.

The multilayered catalysts were synthesized similarly to the model catalysts; however, the incipient wetness impregnation of the group 5–7 transition metal oxide overlayer was added to an existing calcined alumina-, titania-, and zirconia-surface modified SiO_2 support. The calcination procedures followed that for the model catalysts for the corresponding systems. The CrO_3, MoO_3, WO_3, and Re_2O_7 on the surface modified SiO_2 supports were synthesized at 3 wt% (with V_2O_5 synthesized at 5 wt%, in keeping with earlier studies) unless specified otherwise and are designated as $M_1O_x/M_2O_x/SiO_2$ (e.g., $CrO_3/Al_2O_3/SiO_2$).

2.2. CH_3OH-TPSR spectroscopy

The surface reactivity of the model supported MO_x/SiO_2 and multilayered supported $M_1O_x/M_2O_x/SiO_2$ catalysts was determined by CH_3OH-TPSR spectroscopy. CH_3OH is a "smart" chemical probe molecule that distinguishes among surface acidic, redox, and basic sites [24]. The dissociative chemisorption of methanol forms surface methoxy (CH_3O^*) intermediate species, the most abundant reaction intermediate (MARI) [31,32]. The surface methoxy intermediate undergoes different reaction pathways that depend the nature of the catalytic active site: formaldehyde (HCHO) from redox sites, dimethyl ether (CH_3OCH_3, DME) from acidic sites, and CO/CO_2 from basic sites [24,33]. No additional reaction products, such as methyl formate (MF) and dimethoxy methane (DMM), were found in the present study. Formation of H_2O always accompanies the CH_3OH surface chemistry, but this was not evaluated in the study because it does not provide any additional insight. In addition, the formation of CO was not explicitly investigated because of its similarity to the CO_2 combustion product.

The CH_3OH-TPSR spectra were obtained with a commercial TPSR system (Altamira Instruments, AMI-200) equipped with an on-line quadrupole mass spectrometer (Ametek Dycor Dymaxion with Dycor System 2000 software). The catalyst samples, typically 200–300 mg of loose powder, were placed in a quartz bubble U-tube and held in place by glass wool. The U-tube was placed in a clamshell furnace capable of linear heating rates from 1-30 °C/min up to 1200 °C, with the temperatures measured by thermocouples both at the top of the sample bed and at the center of the furnace. The gas flow, accurately metered by mass flow controllers (Brooks, model 5850E series), and the temperature setpoints were fully computer-automated (controlled by a LabVIEW-based application software). The exhaust line from the U-tube reactor to the mass spectrometer (MS) was maintained at ∼100 °C to prevent condensation of the methanol and reaction products. The typical protocol for obtaining the CH_3OH-TPSR spectra was as follows. The samples were first pretreated at 450 °C under flowing air (Airgas, Zero grade) for 1 h at 30 sccm, then cooled to 110 °C to prevent moisture condensation. The flowing gas was switched to helium (Airgas, UHP) as the samples were allowed to cool further to 100 °C for 30 min to remove any physically adsorbed oxygen. Then a CH_3OH/He (Airgas, Certified, 2000 ppm CH_3OH/He) gas mixture was introduced and chemisorbed at 100 °C (30 sccm) for 30–45 min, depending on the catalyst weight [24, 34]. A methanol breakthrough curve was obtained with the MS for each run to ensure saturation of the catalyst surface. The catalyst samples were purged with helium for 1 h to remove physically adsorbed methanol, and then the sample temperature was ramped at 10 °C/min from room temperature to 500 °C under either helium or blended 1% O_2/He (Airgas, Certified, 9.735% O_2/He) gas. The 1% O_2/He carrier flow was used for the easily reducible supported metal oxide systems because reduction produces a second, high-temperature TPSR peak from the reduced sites, and the 1%

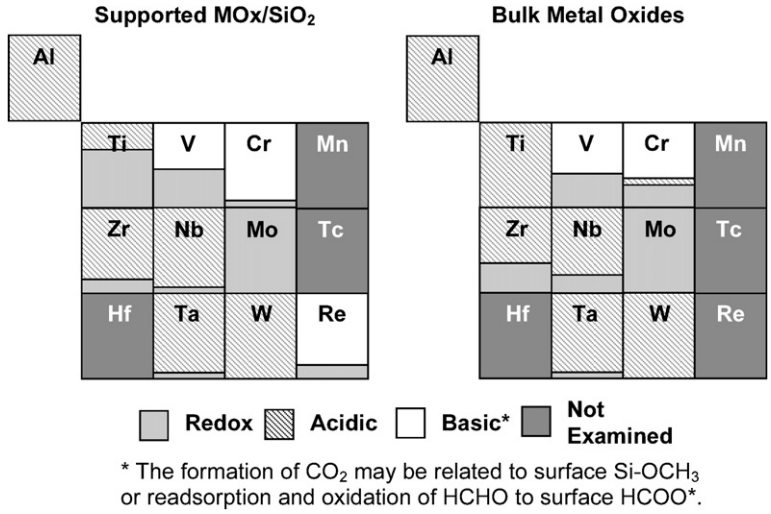

Fig. 1. CH_3OH-TPSR relative selectivity of supported MO_x/SiO_2 (left) at maximum attainable surface metal oxide coverage, without the presence of crystalline MO_x NPs, and their corresponding bulk MO_x (right). The volatile nature of bulk Re_2O_7 prevented the study of this unsupported MO_x.

O_2/He mixture prevents surface reduction and provides MS spectra for the fully oxidized surface metal oxides.

The m/e^- values used to detect the various TPSR products were $m/e^- = 30$ (primary) and 29 (secondary) for HCHO, $m/e^- = 45$ (primary) and 46 (secondary) for CH_3OCH_3 (DME), $m/e^- = 31$ for CH_3OH, $m/e^- = 28$ for CO, and $m/e^- = 44$ for CO_2. In addition, reaction-limited CH_3OH also was formed at $T_p \sim 170$–$200\,°C$ from the recombination of the surface CH_3O^* and H^* species. The low T_p value indicates the ease at which the recombination occurred, whereas previous transient kinetic isotopic studies with CH_3OH and CD_3OD revealed the efficient formation of CH_3OD and CD_3OH species [35]. The contribution of the HCHO cracking fraction of CH_3OH was carefully subtracted out of the apparent HCHO MS signal when it overlapped with the true HCHO signal. The relative selectivity toward each desorption product was determined from the areas under the TPSR curves using a Lorentzian fit.

The surface kinetic parameters (E_{act} and k_{rds}) for the surface methoxy reactions to HCHO, CH_3OCH_3, and CO/CO_2 were obtained directly from the CH_3OH-TPSR spectra. The RDS for the unimolecular surface CH_3O^* dehydrogenation to HCHO involves breaking the surface methoxy C–H bond [33]. The RDS for CH_3OCH_3 formation involves unimolecular surface methoxy C–O bond scission [26,36]. Formation of CO/CO_2 proceeds through conversion of the surface CH_3O^* to surface formate ($HCOO^*$), and the RDS involves breaking either the surface formate C–H or C–O bond unimolecular reactions [25]. The unimolecular aspect of the RDS for the different reaction pathways allows application of the first-order Redhead equation [37] to determine the E_{act} for the surface reactions,

$$\frac{E_{act}}{RT_p^2} = \left(\frac{\nu}{\beta}\right)\exp\left(\frac{-E_{act}}{RT_p}\right), \tag{1}$$

in which T_p is the CH_3OH-TPSR peak temperature of the reaction product, R is the gas constant (1.987 cal/mol K), $\nu = 10^{13}\ s^{-1}$ for first-order kinetics [34], and β is the heating rate (10 °C/min). The RDS of the surface methoxy intermediate conversion to DME and HCHO, k_{rds}, is a function of E_{act} (and hence T_p) and is determined by

$$k_{rds} = \nu \exp\left(\frac{-E_{act}}{RT}\right), \tag{2}$$

in which T is a reference temperature used for the comparison of k_{rds} values. In keeping with previous investigations, this study also used $T = 230\,°C$ as the reference temperature.

3. Results

3.1. Model supported MO_x/SiO_2 catalysts

The CH_3OH-TPSR spectrum of the pure SiO_2 reflects the relatively low reactivity of the native SiO_2 support and the absence of any significant surface redox (HCHO formation), acidic (DME formation), and basic (CO_2 formation) sites (see Supporting Information, Fig. S1). The model SiO_2-supported metal oxide catalyst samples used in the present study (AlO_x/SiO_2, TiO_x/SiO_2, ZrO_x/SiO_2, VO_x/SiO_2, NbO_x/SiO_2, TaO_x/SiO_2, CrO_x/SiO_2, MoO_x/SiO_2, WO_x/SiO_2, and ReO_x/SiO_2) were previously shown to be 100% dispersed as surface oxides on the SiO_2 support by Raman, IR, UV–vis, XANES, and solid-state ^{51}V and ^{27}Al NMR spectroscopy [21–23,38–52]. The CH_3OH-TPSR spectra of the model SiO_2 catalyst systems reveal that adding the surface metal oxides introduced surface redox, acidic, and basic catalytic active sites (see Supporting Information, Figs. S2–S11). The peak temperature, T_p, and k_{rds} of the model supported MO_x/SiO_2 catalytic systems for the formation of DME (see Table 1), HCHO, and CO_2 (see Table 2), along with the relative peak area ratios of HCHO:DME:CO_2 (see Table 3) for each system, are summarized below. The selectivity and k_{rds} information are plotted in Figs. 1 and 2, to facilitate visual inspection of the data. The corresponding E_{act} values are tabulated elsewhere (see Supporting Information, Table S1). In general, the CH_3OH-TPSR spectral intensity of the reaction products for each supported MO_x/SiO_2 system increased with surface MO_x coverage and decreased slightly in T_p with surface coverage. The increase in MS signal intensity (area under the TPSR curve) was proportional to the number of catalytic active sites, and the slight drop in T_p values was related to the decreased concentration of the less reactive surface Si–OCH_3 intermediates with increasing surface MO_x coverage. A decrease in the T_p corresponds to a decrease in E_{act} and an increase in k_{rds}.

Figs. 1 and 2 also compare the selectivity and activity from the CH_3OH-TPSR studies of the model supported MO_x/SiO_2 catalysts with those of their corresponding unsupported, bulk MO_x catalysts. The selectivity patterns of the surface MO_x catalytic active sites on SiO_2 were comparable to those of their corresponding bulk MO_x oxides, with one exception: The supported TiO_2/SiO_2 catalyst system exhibited significant redox character in addition to DME formation, whereas the bulk TiO_2 system yielded DME exclusively. With few exceptions, the bulk MO_x catalysts tended to be more active than their corresponding SiO_2-supported surface MO_x species. The difference reflects the changes associated with

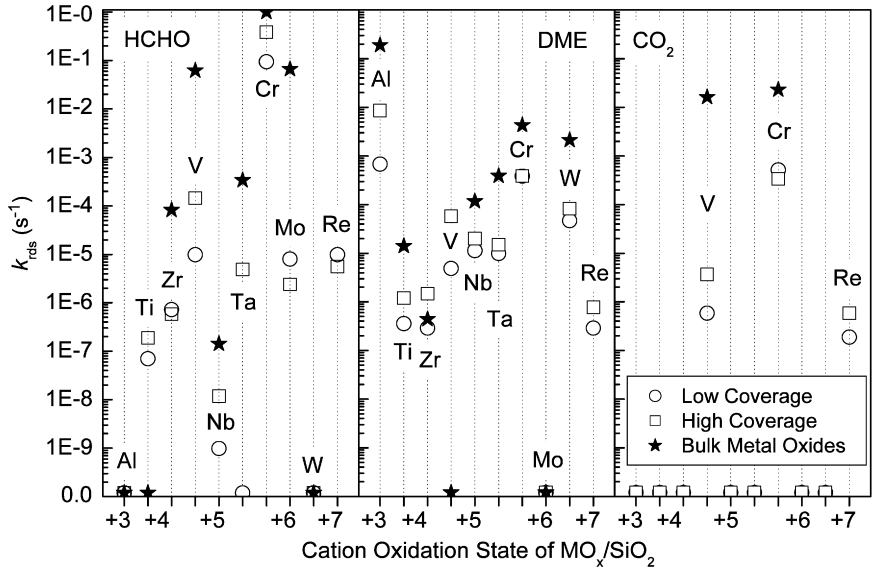

Fig. 2. k_{rds} of HCHO, DME and CO_2 of MO_x/SiO_2 at 230 °C for low and high (maximum dispersion) metal oxide coverage. The k_{rds} values of bulk oxides are shown for reference with notation as stars [24–27].

anchoring the isolated surface MO_x species on the SiO_2 surface. In general, the SiO_2-supported MO_x species had comparable selectivity to and slightly lower surface reactivity than their bulk MO_x counterparts.

The k_{rds} (DME) trends for the model supported MO_x/SiO_2 metal oxides at low and high maximum dispersion as a function of the metal oxide oxidation state or group number also are shown in Fig. 2. The supported Al_2O_3/SiO_2, CrO_3/SiO_2, and WO_3/SiO_2 systems had the fastest surface kinetics for DME formation and included the most active surface acid sites. The supported TiO_2/SiO_2, ZrO_2/SiO_2, and Re_2O_7/SiO_2 catalysts were two to four orders of magnitude slower in k_{rds} for DME formation; therefore, the k_{rds} values indicate the following periodic group trend of the metal oxide cation oxidation state: (+3) > (+6) > (+5) > (+4) ∼ (+7). Each group in this trend was approximately one order of magnitude greater than the next, starting with the fastest k_{rds} (DME) for supported Al_2O_3/SiO_2. The k_{rds} values also were generally higher at higher metal oxide loading, and the periodic group trend held true for all loading coverages. The k_{rds} (DME) values for the bulk oxides of Al_2O_3, TiO_2, ZrO_2, Nb_2O_5, Ta_2O_5, Cr_2O_3, and WO_3, indicated by the star symbol in Fig. 2 were slightly greater (within one order of magnitude) than their corresponding SiO_2-supported oxides [24]. Only the bulk V_2O_5 and MoO_3 bulk metal oxides did not exhibit activity for DME formation during CH_3OH-TPSR.

The k_{rds} trends for the formation of HCHO of the model MO_x/SiO_2 systems also are shown in Fig. 2 for the same surface metal oxide coverages. The supported CrO_3/SiO_2 system had the most active surface redox catalytic sites, and its k_{rds} value was approximately three orders of magnitude greater than those for the supported V_2O_5/SiO_2, Re_2O_7/SiO_2, and MoO_3/SiO_2 systems. The bulk oxides of ZrO_2, V_2O_5, Nb_2O_5, Ta_2O_5, Cr_2O_3, and MoO_3 and their k_{rds} (HCHO) values, indicated by the star symbol in Fig. 2, generally were several orders of magnitude greater than their corresponding SiO_2-supported oxide catalysts. Only the bulk Al_2O_3, TiO_2, and WO_3 systems did not give rise to HCHO formation during CH_3OH-TPSR. The least active redox catalytic sites were found for the supported TiO_2/SiO_2, ZrO_2/SiO_2, and Nb_2O_5/SiO_2 catalysts, which were another order of magnitude lower in k_{rds} (HCHO).

Only the supported V_2O_5/SiO_2, CrO_3/SiO_2, and Re_2O_7/SiO_2 catalysts gave rise to CO_2 production (see Figs. 1 and 2). Although CO_2 formation is reflective of basic catalytic active sites, CO_2 formation also can arise from decomposition of surface Si–OCH_3 intermediates and readsorption/oxidation of the HCHO reaction product. Note that these supported catalysts also have active redox sites for HCHO production. We do not discuss CO_2 formation further here, because of the uncertain nature of the origin of CO_2 production.

Table 1
CH_3OH-TPSR surface kinetics (k_{rds}) of model supported MO_x/SiO_2 catalysts (M = Al, Ti, Zr, V, Nb, Ta, Cr, Mo, W, and Re) for surface methoxy dehydration to DME

Wt (%)	T_p (°C)	k_{rds} (DME) (s^{-1})	T_p (°C)	k_{rds} (DME) (s^{-1})	T_p (°C)	k_{rds} (DME) (s^{-1})	T_p (°C)	k_{rds} (DME) (s^{-1})
	Al_2O_3/SiO_2							
1	270	6.82E−4						
3	248	3.21E−3						
5	241	5.26E−3						
10	234	8.60E−3						
	TiO_2/SiO_2		V_2O_5/SiO_2		CrO_3/SiO_2			
1	377	3.56E−7	340	4.88E−6	278	3.88E−4		
3					278	3.88E−4		
5	372	5.07E−7	330	9.89E−6				
8	364	8.93E−7						
10			310	4.06E−5				
12	360	1.19E−6	285	2.37E−4				
	ZrO_2/SiO_2		Nb_2O_5/SiO_2		MoO_3/SiO_2			
1	380	2.88E−7	328	1.14E−5	–	–		
5	378	3.31E−7	326	1.31E−5				
8	357	1.47E−6	324	1.51E−5				
10	360	1.19E−6	320	2.00E−5	–	–		
15	357	1.47E−6						
			Ta_2O_5/SiO_2		WO_3/SiO_2		Re_2O_7/SiO_2	
1			330	9.89E−6	330	9.89E−6	–	–
3					308	4.68E−5	380	2.88E−7
5			330	9.89E−6	295	1.17E−4	366	7.75E−7
6					300	8.23E−5		
8			324	1.51E−5				
10			324	1.51E−5				

3.2. Multilayered supported $M_1O_x/M_2O_x/SiO_2$ catalysts

The surface chemistry and kinetics of the group 5–7 surface metal oxides (VO_x, CrO_x, MoO_x, WO_x, and ReO_x) on the alumina-, titania-, and zirconia-surface modified SiO_2 supports were also chemically probed with CH_3OH-TPSR. The resulting catalytic activity and selectivity patterns are shown in Figs. 3 and 4, respectively, and the k_{rds} values are listed in Table 4 (also see Supporting Infor-

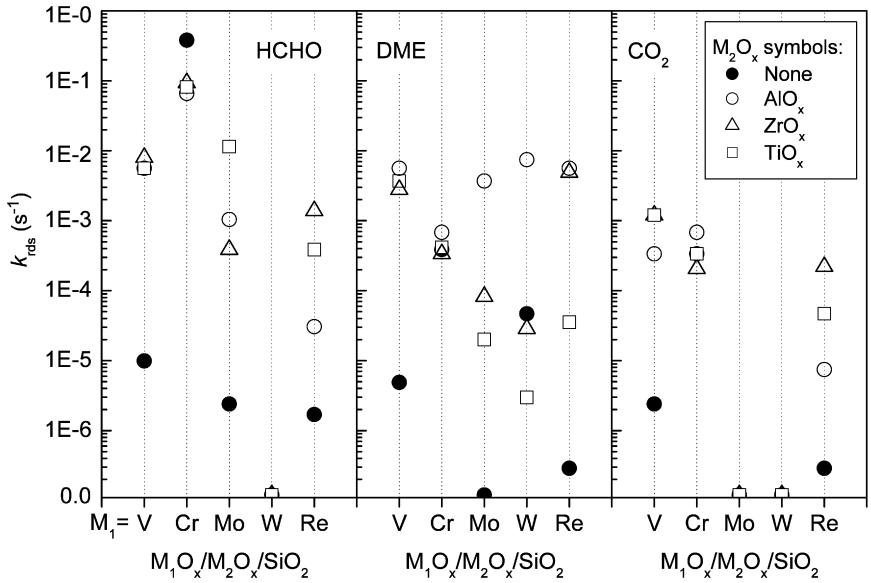

Fig. 3. k_{rds} of supported 3%M_1O_x/5%M_2O_x/SiO_2 (M_1 = V, Cr, Mo, W, and Re; M_2 = Al, Zr, and Ti, with exception of V_2O_5 at 5%) for surface methoxy decomposition to DME, HCHO, and CO_2.

Table 2
CH_3OH-TPSR surface kinetics (k_{rds}) of model supported MO_x/SiO_2 catalysts (M = Al, Ti, Zr, V, Nb, Ta, Cr, Mo, W, and Re) for surface methoxy dehydrogenation to HCHO (left columns) and formation of CO_2 (right column)

Wt (%)	T_p (°C)	k_{rds} (HCHO) (s^{-1})	T_p (°C)	k_{rds} (HCHO) (s^{-1})	T_p (°C)	k_{rds} (HCHO) (s^{-1})	T_p (°C)	k_{rds} (HCHO) (s^{-1})	T_p (°C)	k_{rds} (CO_2) (s^{-1})
	Al_2O_3/SiO_2[a]									
1	–	–								
3	–	–								
5	–	–								
10	–	–								
	TiO_2/SiO_2[a]		V_2O_5/SiO_2		CrO_3/SiO_2				V_2O_5/SiO_2	
1	400	6.98E−8	345	3.42E−6	200	9.38E−2			370	5.84E−7
3					183	3.82E−1				
5	418	1.95E−8	330	9.89E−6					350	2.40E−6
8	386	1.88E−7								
10			305	5.78E−5					346	3.19E−6
12	386	1.88E−7	292	1.45E−4					344	3.68E−6
	ZrO_2/SiO_2[a]		Nb_2O_5/SiO_2[a]		MoO_3/SiO_2[a]				CrO_3/SiO_2	
1	–	–	460	9.87E−10	333	8.00E−6			274	5.15E−4
3					350	2.40E−6			280	3.37E−4
5	367	7.22E−7	455	1.41E−9						
8	356	1.57E−6	445	2.86E−9						
10	370	5.84E−7	425	1.18E−8	350	2.40E−6				
15	370	5.84E−7								
			Ta_2O_5/SiO_2[a]		WO_3/SiO_2[a]		Re_2O_7/SiO_2		Re_2O_7/SiO_2	
1			–	–	–	–	330	9.89E−6	386	1.88E−7
3			–	–	–	–	355	1.69E−6	380	2.88E−7
5					–	–	338	5.62E−6	370	5.84E−7
8			338	5.62E−6						
10			340	4.88E−6						

[a] Denotes catalytic system with no formation of CO_2 product below 500 °C.

mation Figs. S12–S16 for CH_3OH-TPSR spectra and T_p values and Table S2 for E_{act} values). With the exception of the surface AlO_x modifier, which dominates the acidic character of the catalysts, the selectivity of the multilayered catalysts are mainly comparable to the model supported MO_x/SiO_2 catalysts without the surface modifiers. The presence of the surface modifiers generally enhanced the activity of the surface VO_x, MoO_x, and ReO_x redox sites and depressed the activity of surface WO_x acid sites. The DME formation for multilayered catalysts with surface AlO_x modifiers was not taken into consideration because of the significant contribution of the surface AlO_x sites to DME production.

The HCHO formation k_{rds} values for the multilayered supported catalysts, as shown in Fig. 3, exhibited significantly enhanced surface reactivity compared with the model reference supported systems (represented by the black circles) for the redox supported V_2O_5/SiO_2, MoO_3/SiO_2, and Re_2O_7/SiO_2 catalysts. The surface modifiers increased k_{rds} (HCHO) by one to three orders of magnitude, with the exception of the supported chromia system, which was not significantly affected and decreased slightly in activity. These results agree well with findings from previous steady-state CH_3OH oxidation studies in which the turnover frequency (TOF) [53] increased by more than an order of magnitude with addition of the surface modifiers for HCHO formation [1–3,54]. CH_3OH oxi-

dation steady-state reaction studies for supported $CrO_3/TiO_x/SiO_2$ confirmed that the TOF and selectivity toward HCHO did not differ appreciably from those for the model CrO_3/SiO_2 system [55]. The enhanced redox activity did not originate from the less active surface titania or zirconia sites, because these formed HCHO at higher temperatures ($T_p > 350\,°C$). The surface modifiers did not appreciably affect the redox character of the supported tungsta systems, because they generally did not yield HCHO, with the exception of the supported $WO_3/TiO_x/SiO_2$ catalyst, which created weak redox surface sites at a high $T_p \sim 436\,°C$.

The DME formation k_{rds} for the multilayered supported metal oxide catalysts, as shown in Fig. 3, also were strongly influenced by addition of the surface modifiers. The presence of the very active surface AlO_x sites appeared to dominate the overall acidity; consequently, the AlO_x-containing multilayered catalyst systems cannot be considered in any analysis. In contrast, the supported ZrO_x and TiO_x sites exhibited surface acidic sites that were relatively unreactive and produced DME only at elevated temperatures, above those seen for the group 5–7 supported metal oxides. The surface modifiers dramatically enhanced the DME formation kinetics of the both surface VO_x (T_p from ∼330–340 °C to ∼235–250 °C with k_{rds}

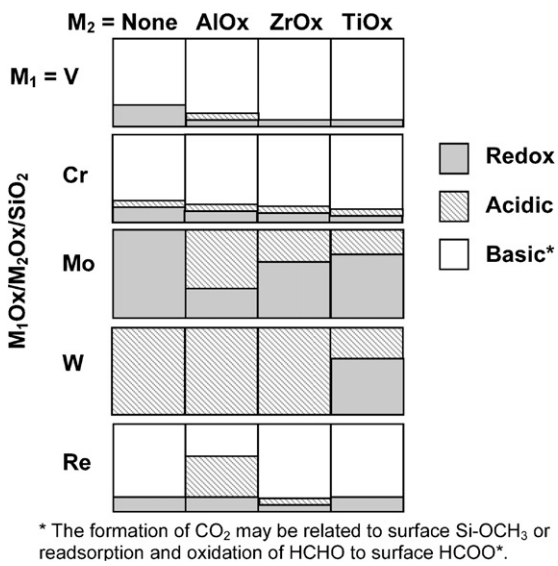

Fig. 4. CH_3OH-TPSR relative selectivity of supported $3\%M_1O_x/5\%M_2O_x/SiO_2$ (except V_2O_5 with 5%) for multilayered catalysts. M_1 represent the group 5–7 transition metal oxides and M_2 represents surface AlO_x, TiO_x and ZrO_x. The column labeled none indicates that no surface M_2O_x species have been added.

Table 3
HCHO:DME:CO_2 ratios for model supported MO_x/SiO_2 catalysts

Wt (%)	HCHO:DME:CO_2 ratio (A_{HCHO}:A_{DME}:A_{CO_2})			
	Al_2O_3/SiO_2			
1	0:1:0			
3	0:1:0			
5	0:1:0			
10	0:1:0			
	TiO_2/SiO_2	V_2O_5/SiO_2	CrO_3/SiO_2	
1	4:1:0	8:1:27	3:1:45	
3			2:1:60	
5	3:1:0	20:1:35		
8	2:1:0			
10		25:1:37		
12	2:1:0	24:1:33		
	ZrO_2/SiO_2	Nb_2O_5/SiO_2	MoO_3/SiO_2	
1	0:1:0	0.20:1:0	1:0:0	
3			1:0:0	
5	0.20:1:0	0.13:1:0		
8	0.20:1:0	0.08:1:0	1:0:0	
10	0.20:1:0	0.08:1:0		
15	0.17:1:0			
		Ta_2O_5/SiO_2	WO_3/SiO_2	Re_2O_7/SiO_2
1		0:1:0	0:1:0	1:0:9
3			0:1:0	13:1:98
5		0:1:0	0:1:0	12:1:90
6			0:1:0	
8		0.07:1:0		
10		0.07:1:0		

Table 4
CH_3OH-TPSR surface kinetics (k_{rds}) of supported $3\%M_1O_x/5\%M_2O_x/SiO_2$ (M_1 = V, Cr, Mo, W, and Re; M_2 = Al, Zr, and Ti, with exception of V_2O_5 at 5%) for surface methoxy decomposition to DME, HCHO, and CO_2. The peak area ratio of HCHO:DME for each system is also listed

	$M_1O_x/M_2O_x/SiO_2$ multilayered catalyst systems									
	T_p (°C)	k_{rds} (s^{-1})	T_p (°C)	k_{rds} (s^{-1})	T_p (°C)	k_{rds} (s^{-1})	T_p (°C)	k_{rds} (s^{-1})	T_p (°C)	k_{rds} (s^{-1})
M_2O_x	$M_1O_x = V_2O_5$		CrO_3		MoO_3		WO_3		Re_2O_7	
DME										
None	340	4.88E−6	278	3.88E−4	–	–	308	4.68E−5	380	2.88E−7
AlO_x	240	5.64E−3	270	6.82E−4	246	3.70E−3	236	7.47E−3	240	5.64E−3
ZrO_x	250	2.79E−3	280	3.37E−4	300	8.23E−5	315	2.85E−5	242	4.90E−3
TiO_x	246	3.70E−3	277	4.17E−4	320	2.00E−5	347	2.97E−6	312	3.53E−5
HCHO										
None	330	9.89E−6	183	3.82E−1	350	2.40E−6	–	–	355	1.69E−6
AlO_x	240	5.64E−3	205	6.60E−2	264	1.04E−3	–	–	314	3.06E−5
ZrO_x	235	8.02E−3	200	9.38E−2	278	3.88E−4	–	–	260	1.38E−3
TiO_x	240	5.64E−3	202	8.15E−2	230	1.14E−2	436	5.43E−9	278	3.88E−4
CO_2										
None	350	2.40E−6	280	3.37E−4	–	–	–	–	380	2.88E−7
AlO_x	280	3.37E−4	270	6.82E−4	–	–	–	–	334	7.45E−6
ZrO_x	262	1.20E−3	287	2.06E−4	–	–	–	–	286	2.21E−4
TiO_x	262	1.20E−3	280	3.37E−4	–	–	–	–	308	4.68E−5
HCHO:DME:CO_2 ratio (A_{HCHO}:A_{DME}:A_{CO_2})										
None	20:1:58		2:1:42		1:0:0		0:1:0		13:1:82	
AlO_x	2:1:18		2:1:60		0.5:1:0		0:1:0		0.33:1:1	
ZrO_x	18:1:150		2:1:70		2:1:0		0:1:0		1:1:10	
TiO_x	7:1:54		2:1:90		4:1:0		2:1:0		8:1:52	

increasing from $\sim 10^{-6}$ to $\sim 10^{-3}$ s^{-1}) and surface ReO_x (T_p decreases from ∼380 to ∼240 °C and k_{rds} increasing from $\sim 10^{-7}$ to $\sim 10^{-3}$ s^{-1}) species. For the supported MoO_x systems, the surface modifiers created surface acidic character that were absent on the model system, possibly originating from the surface ZrO_x and TiO_x sites. The surface modifiers did not appear to appreciably affect the acidic behavior of the supported chromia and tungsta systems. CH_3OH oxidation steady-state reaction studies for $CrO_3/TiO_x/SiO_2$ confirmed that the TOF and selectivity toward DME were not appreciably different from those for the model supported CrO_3/SiO_2 catalyst [55].

4. Discussion

4.1. Model supported M_1O_x/SiO_2 catalysts

The selectivity pattern of the model silica-supported surface M_1O_x catalytic active sites during CH_3OH-TPSR was similar to that of the corresponding unsupported, bulk M_1O_x transition metal oxides (see Fig. 1). This similarity indicates that the intrinsic redox, acidic, and basic characteristics of each transition metal oxide were retained when anchored onto the SiO_2 surface. One exception to this trend is the supported TiO_x species, which exhibited significant redox character compared with bulk TiO_2, dominated by its acidic character. Additional characterization studies are needed to fully understand the origin of the enhanced redox characteristics of the surface TiO_x species on SiO_2.

The selectivity trend is related to the known inorganic chemistry properties of the bulk metal oxides [56]. First, the first-row transition metal oxides (TMOs) were more easily reducible than the second- and third-row TMOs [56], which qualitatively suggests that the first-row transition metal oxides will be more active for oxidation reactions. As demonstrated earlier, VO_x was more active and more reducible than NbO_x and TaO_x, and CrO_x was more active and reducible than both MoO_x and WO_x. Second, the redox properties were enhanced with the transition metal oxide oxidation state ($+4 < +5 < +6 < +7$) [56]. As shown in Fig. 2, the redox k_{rds} values increased as $Ti^{+4} < V^{+5} < Cr^{+6}$ for the first-row TMOs, as $Zr^{+4} \sim Nb^{+5} < Mo^{+6}$ for the second-row TMOs, and as $Ta^{+5} < W^{+6} < Re^{+7}$ for the third-row TMOs. These redox reactivity values for the supported MO_x/SiO_2 catalysts correlate well with the periodic trends from inorganic chemistry properties.

Combining the molecular structural information [21] with the current CH_3OH-TPSR chemical probe study findings allows us to examine possible structure–activity relationships for the model group 4–7 supported MO_x/SiO_2 catalysts. It does not appear that the local molecular structure of the surface MO_x species on SiO_2 was the dominant factor in determining the surface redox, acidic, and basic characteristics. For example, although the group 5 supported metal oxide catalysts (V_2O_5/SiO_2, Nb_2O_5/SiO_2, Ta_2O_5/SiO_2) exhibited the same surface molecular structure, an isolated monoxo $O{=}M(-O-Si)_3$ structure, the surface VO_x was dominated by redox characteristics, whereas the surface NbO_x and TaO_x were primarily acidic sites. Similarly, although the group 6 supported metal oxide catalysts (CrO_3/SiO_2, MoO_3/SiO_2, and WO_3/SiO_2) had the same surface molecular structures of predominantly isolated dioxo $(O{=})_2M(-O-Si)_2$ species, the three systems exhibited different reactivity characteristics. Therefore, the local structure of the dehydrated surface MO_x species on SiO_2 does not appear to determine the surface reactivity of the catalytic active sites.

However, the surface reactivity of the model silica-supported M_1O_x catalytic active sites, as chemically probed by CH_3OH-TPSR, was affected by anchoring of the M_1O_x transition metal oxides to the SiO_2 support. The activity of the surface M_1O_x catalytic active sites on SiO_2 was generally lower than that of their unsupported, bulk M_1O_x transition metal oxides. Although some contribution may come from the different molecular structures of the silica-supported M_1O_x species compared with their unsupported M_1O_x counterparts, the major effect on the surface M_1O_x species appears to be their coordination to the silica support, which has a high cation electronegativity [57].

4.2. Multilayered supported $M_1O_x/M_2O_x/SiO_2$ catalysts

The addition of the surface modifiers in the multilayered supported metal oxide catalysts generally did not significantly alter the CH_3OH-TPSR product selectivity (see Fig. 4). The acidic supported $WO_3/TiO_2/SiO_2$ catalyst exhibited some redox character with the addition of surface TiO_x, and the redox supported $MoO_3/ZrO_2/SiO_2$ and $MoO_3/TiO_2/SiO_2$ catalyst systems exhibited some acidic character with the addition of surface ZrO_x and TiO_x. Consequently, the surface M_1O_x catalytic active sites in the multilayered supported $M_1O_x/M_2O_x/SiO_2$ catalysts were found to mostly retain their intrinsic chemical properties, because the product selectivity demonstrated no appreciable change from the introduction of the surface modifiers.

The introduction of surface AlO_x, TiO_x, and ZrO_x modifiers onto the SiO_2-support dramatically enhanced the k_{rds} redox values (by as much as a factor of $\sim 10^4$) of the supported M_1O_x catalytic active sites. All of the multilayered supported $VO_x/M_2O_x/SiO_2$ and $ReO_x/M_2O_x/SiO_2$ catalyst systems contained the same surface monoxo VO_4 and trioxo ReO_4 structures, respectively. Thus, the enhanced redox reactivity cannot be related to local molecular structural changes, but instead must be a consequence of the ligand effect of the different substrate cations (Si, Al, Ti, and Zr). We propose that the enhanced redox activity is related to the lower electronegativity of substrate cations, Si > Al > Ti ∼ Zr, which inversely affects the electron density on the bridging V–O-support bond. Several recent theoretical DFT/ab initio calculations have concluded that for supported vanadia catalytic systems, the bridging V–O-support bond is the most energetically favorable methanol chemisorption site on the surface VO_x structure [51,58–60]. The inverse surface reactivity trend with cation electronegativity also was seen for the acidic sites of the multilayered supported $WO_3/M_2O_x/SiO_2$ catalyst systems. For the acidic surface WO_x catalytic active sites, the fewer the number of electronegative cations introduced, the greater the resulting electron density on the bridging W–O-support bonds, which appeared to mildly suppress their acidic activity rather than produce catalytic enhancement. Similarly for the basic multilayered supported $CrO_3/M_2O_x/SiO_2$ catalysts, introduction of the less electronegative surface Al, Zr, and Ti cations had only a minor effect on the overall reactivity. Thus, the surface AlO_x, ZrO_x, and TiO_x modifiers appear to have the most pronounced catalytic enhancing effect on the surface redox catalytic active sites on SiO_2.

5. Conclusion

In this work, the surface reactivity of model supported M_1O_x/SiO_2 and multilayered supported $M_1O_x/M_2O_x/SiO_2$ catalysts (where M_1 represents the group 5–7 transition metal oxides and M_2 represents Al, Zr, or Ti) were chemically probed by CH_3OH-TPSR spectroscopy. For the model supported M_1O_x/SiO_2 catalysts, the k_{rds} activity trend was seen to follow the periodic trends for inorganic chemistry properties; the first-row transition metal oxides were more easily reducible than the second- and third-row metal oxides, and redox activity increased with oxidation state ($+4 < +5 < +6 < +7$). The inverse trend was found to hold for the acidic activity of the model supported MO_x/SiO_2 catalysts. For the multilayered supported $M_1O_x/M_2O_x/SiO_2$ catalytic systems, the surface M_2O_x modifiers had no significant effect on the selectivity

of the surface M_1O_x catalytic active sites, but the surface modifiers did have a significant effect on the catalytic activity of the SiO_2-supported metal oxide catalysts. The k_{rds} activity of the redox surface vanadia, molybdena, and rhenia catalytic active sites was enhanced by $\sim 10^1$–10^4. The presence of the surface modifiers only mildly perturbed the reactivity of the basic surface CrO_x sites, but suppressed the reactivity of the acidic surface WO_x catalytic actives sites. In general, the selectivity was controlled by the intrinsic properties of each surface M_1O_x site, and the surface reactivity was significantly influenced by the anchoring surface M_2O_x ligands. Thus, the catalytic activity was controlled by the M_2O_x ligand according to the electronic requirements of the different reaction pathways and the electronegativity (Si > Al > Ti ∼ Zr) of the anchoring sites or ligands.

Acknowledgments

Funding for this study was provided by the U.S. Department of Energy, Basic Energy Sciences (grant DE-FG02-93ER14350).

Supplementary material

The online version of this article contains additional supplementary material: Tables S1–S2 and Figs. S1–S16.

Please visit DOI: 10.1016/j.jcat.2008.06.002.

References

[1] X. Gao, I.E. Wachs, J. Catal. 192 (2000) 18.
[2] X. Gao, J.L.G. Fierro, I.E. Wachs, Langmuir 15 (1999) 3169.
[3] X. Gao, S.R. Bare, J.L.G. Fierro, I.E. Wachs, J. Phys. Chem. B 103 (1999) 618.
[4] B.N. Reddy, M. Subrahmanyam, Langmuir 8 (1992) 2072.
[5] R. Mariscal, M. Galan-Fereres, J.A. Anderson, L.J. Alemany, J.M. Palacios, J.L.G. Fierro, in: G. Centi, C. Cristiani, P. Forzatti, S. Perathoner (Eds.), Environmental Catalysis, SCI, Rome, 1995, p. 223.
[6] M.D. Amiridis, J.P. Solar, Ind. Eng. Chem. Res. 35 (1996) 978.
[7] R.A. Rajadhyaksha, G. Hausinger, H. Zeilinger, A. Ramstetter, H. Schmeiz, H. Knözinger, Appl. Catal. 51 (1989) 67.
[8] R.A. Rajadhyaksha, H. Knözinger, Appl. Catal. 51 (1989) 81.
[9] P. Wauthoz, T. Machej, P. Grange, Appl. Catal. 69 (1991) 149.
[10] E.T.C. Vogt, A. Boot, A.J. van Dillen, J.W. Geus, F.J.J.G. Janssen, F.M.G. van den Kerkhof, J. Catal. 114 (1988) 313.
[11] M. Galan-Fereres, R. Mariscal, L.J. Alemany, J.L.G. Fierro, J. Chem. Soc. Faraday Trans. 90 (1994) 3711.
[12] M.P. McDaniel, M.B. Welsh, M.J. Dreiling, J. Catal. 82 (1983) 98.
[13] S.J. Conway, J.W. Falconer, C.H. Rochester, J. Chem. Soc. Faraday Trans. 85 (1989) 71.
[14] S. Rajagopal, T.L. Grimm, D.J. Collins, R. Miranda, J. Catal. 137 (1992) 453.
[15] M. Henker, K.P. Wendlandt, J. Valyon, P. Bornmann, Appl. Catal. 69 (1991) 205.
[16] S. Damyanova, A. Docteva, C. Vladov, L. Petrov, P. Grange, B. Delmon, Belg. Chem. Commun. 30 (1999) 306.
[17] S. Damyanova, M.A. Centeno, L. Petrov, P. Grange, Spectrochim. Acta A 57 (2001) 2495.
[18] B.M. Reddy, B. Chowdhury, P.G. Smirniotis, Appl. Catal. A 211 (2001) 19.
[19] J.A. Moulijn, J.C. Mol, J. Mol. Catal. 46 (1988) 1.
[20] D. Mandelli, M.C.A. van Vliet, U. Arnold, R.A. Sheldon, U. Schuchardt, J. Mol. Catal. A 168 (2001) 165.
[21] E.L. Lee, I.E. Wachs, J. Phys. Chem. C 111 (2007) 14410.
[22] E.L. Lee, I.E. Wachs, J. Phys. Chem. C 112 (2008) 6487.
[23] E.L. Lee, I.E. Wachs, J. Phys. Chem. C, submitted for publication.
[24] M. Badlani, I.E. Wachs, Catal. Lett. 75 (2001) 137.
[25] X. Wang, I.E. Wachs, Catal. Today 96 (2004) 211.
[26] T. Kim, A. Burrows, C.J. Kiely, I.E. Wachs, J. Catal. 246 (2007) 370.
[27] I.E. Wachs, J.-M. Jehng, W. Ueda, J. Phys. Chem. B 109 (2005) 2275.
[28] X. Gao, S.R. Bare, J.L.G. Fierro, M.A. Banares, I.E. Wachs, J. Phys. Chem. B 102 (1998) 5653.
[29] X. Gao, S.R. Bare, B.M. Weckhuysen, I.E. Wachs, J. Phys. Chem. B 102 (1998) 10842.
[30] J.M. Jehng, I.E. Wachs, J. Phys. Chem. 95 (1991) 7373.
[31] L.J. Burcham, L.E. Briand, I.E. Wachs, Langmuir 17 (2001) 6164.
[32] L.J. Burcham, G. Deo, X. Gao, I.E. Wachs, Top. Catal. 11/12 (2000) 85.
[33] J.M. Tatibouet, Appl. Catal. A 148 (1997) 213.
[34] L.E. Briand, W.E. Farneth, I.E. Wachs, J. Catal. 208 (2002) 301.
[35] J.M. Tatibouet, H. Lauron-Pernot, J. Mol. Catal. A 171 (2001) 205.
[36] I.E. Wachs, T. Kim, E.I. Ross, Catal. Today 116 (2006) 162.
[37] P.A. Redhead, Vacuum 12 (1962) 213.
[38] J.-M. Jehng, W.-C. Tung, C.-H. Huang, I.E. Wachs, Microporous Mesoporous Mater. 99 (2007) 299.
[39] T. Tanaka, H. Nojima, T. Yamamoto, S. Takenaka, T. Funabiki, S. Yoshida, Phys. Chem. Chem. Phys. 1 (1999) 5235.
[40] M. Cornac, A. Janin, J.C. Lavalley, Polyhedron 5 (1986) 183.
[41] C.C. Williams, J.G. Ekerdt, J.-M. Jehng, F.D. Hardcastle, A.M. Turek, I.E. Wachs, J. Phys. Chem. 95 (1991) 8781.
[42] H. Hu, S.R. Bare, I.E. Wachs, J. Phys. Chem. 99 (1995) 10897.
[43] M.A. Banares, H. Hu, I.E. Wachs, J. Catal. 150 (1994) 407.
[44] W. Zhang, A. Desikan, S.T. Oyama, J. Phys. Chem. 99 (1995) 14468.
[45] N. Ohler, A.T. Bell, J. Phys. Chem. B 109 (2005) 23419.
[46] N. Das, H. Eckert, H. Hu, I.E. Wachs, J.F. Walzer, F.J. Feher, J. Phys. Chem. 97 (1993) 8240.
[47] H. Eckert, I.E. Wachs, J. Phys. Chem. 93 (1989) 6796.
[48] M. Baltes, A. Kytokivi, B.M. Weckhuysen, R.A. Schoonheydt, P. van der Voort, E.F. Vansant, J. Phys. Chem. B 105 (2001) 6211.
[49] M.A. Vuurman, I.E. Wachs, D.J. Stufkens, A. Oskam, J. Mol. Catal. 80 (1993) 209.
[50] M.A. Vuurman, D.J. Stufkens, A. Oskam, J. Mol. Catal. 76 (1992) 263.
[51] R.Z. Khaliullin, A.T. Bell, J. Phys. Chem. B 106 (2002) 7832.
[52] B.M. Weckhuysen, I.E. Wachs, R.A. Schoonheydt, Chem. Rev. 96 (1996) 3327.
[53] M. Boudart, Chem. Rev. 95 (1995) 661.
[54] J.-M. Jehng, I.E. Wachs, Catal. Lett. 13 (1992) 9.
[55] J.-M. Jehng, I.E. Wachs, B.M. Weckhuysen, R.A. Schoonheydt, J. Chem. Soc. Faraday Trans. 91 (1995) 953.
[56] N.N. Greenwood, A. Earnshaw, Chemistry of the Elements, Pergamon Press, Elmsford, NY, 1989.
[57] R.T. Sanderson, J. Chem. Educ. 65 (1988) 112.
[58] J.L.Bronkema, A.T. Bell, J. Phys. Chem. C 111 (2007) 420.
[59] J. Dobler, M. Pritzsche, J. Sauer, J. Am. Chem. Soc. 127 (2005) 10861.
[60] N. Magg, B. Immaraporn, J.B. Giorgi, T. Schroeder, M. Baumer, J. Dobler, Z. Wu, E. Kondratenko, M. Cherian, M. Baerns, P.C. Stair, J. Sauer, H.J. Freund, J. Catal. 226 (2004) 88.